A Negative-Curvature Hollow-Core Fiber Structure With Double Trigonal-Symmetrical Anti-Resonant Elements

Yanyan Zhou, Ruiting Cao, Shijie Wang, Jinggang Peng, Haiqing Li, Yingbo Chu, Yingbin Xing, Nengli Dai, and JinYan Li

***Abstract*—We propose a novel negative-curvature hollow-core fiber structure with double trigonal-symmetrical anti-resonant elements implementing single-mode or polarization-maintaining transmission for high-power laser delivery in the 1 μm wavelength window. For the single-mode fiber, the single-mode performance with a higher-order modes extinction ratio (HOMER) as high as $4.65*10^4$ is achieved, and it remains $>1*10^4$ with a large fault tolerance proportion of tubes size, which can increase the flexibility of fiber fabrication. For another polarization-maintaining fiber, an ultra-low confinement loss of 0.005 dB/m is obtained for polarization-maintaining transmission by optimizing the refractive index of the two transverse glass tubes, while the polarization extinction ratio and HOMER remain both $>1*10^3$. This is the first birefringent negative-curvature hollow-core fiber with a loss below 0.01 dB/m in the 1 μm wavelength window.**

***Index Terms*—Negative-curvature hollow-core fibers, single-mode, polarization-maintaining.**

I. Introduction

HIGH power ytterbium doped fiber laser has become the most popular laser source in metal cutting, metal welding and other material processing fields [1]. Single mode fiber lasers with excellent beam quality are expected to achieve high aspect ratio and ultrafast processing speed [2]. While the drawbacks of traditional optical transmission fibers such as nonlinear optical effects and the low material's laser induced damage threshold has hindered the further growing of the high output power [3]. Hollow-core fibers (HCFs) is an ideal medium for ultra-high-power laser transmission with the advantages of lower nonlinearity, and high damage threshold compared with the common solid-core fibers [4]–[7]. The simplified negative-curvature hollow-core fibers (NC-HCFs) with great advantages in bandwidth compared with hollow-core photonic bandgap guiding crystal fibers (HC-PBGFs) [8], as well as simpler structure and lower loss than Kagome hollow-core fibers have attracted much attentions in recent year [9], [10].

The core diameters of NC-HCFs for high power Ytterbium-doped fiber lasers are between 20 and 80 μm [11]–[15]. A large fiber core usually helps to reduce the confinement loss of fundamental mode (FM), while leading to the existence of higher-order modes (HOMs) as well [16]. Breaking this contradiction can further reduce the loss limit of NC-HCFs. And it is beneficial to many fiber lasers applications of high-energy single mode transmission [2]. The inhibited coupling waveguiding mechanism of NC-HCFs points out, the coupling between the core and cladding modes can increase the loss of the core modes, and the coupling is related to the mismatch of their effective indices and field overlap [17]–[20]. Based on the guidance mechanisms, NCs-HCFs can get good single mode performance by means of the reasonable design of the cladding structure for confining the FM to the fiber core and coupling HOMs to the fiber cladding. In 2017, Md Imran Hasan *et al.* [21] showed a nested elliptical element formed NC-HCF with the higher-order mode extinction ratio (HOMER) of LP11 exceeded 1950 at 1.06 μm. Recently, Md. Selim Habib *et al.* [22] proposed a single-mode 5-tube nested NC-HCF with a HOMER ∼12000 at 1.55 μm. However, a small fluctuation of cladding tubes size can have a significant impact on single-mode performance in these high HOMER structures, which means limited flexibility for fibers fabrication. In addition, the design and fabrication of polarization-maintaining NC-HCFs (PM-NC-HCFs) are mainly concentrated in the mid-infrared and THz region [23]–[28], while PM-NC-HCFs in the 1 μm wavelength window have been few reported so far [29], [30].

In this work, we take full advantage of the Inhibited Coupling model and propose a novel NC-HCFs with the double trigonal-symmetrical anti-resonant elements to form a rich variety of cladding modes coupling with different HOMs simultaneously. The higher-order modes extinction ratio (HOMER) of the fiber is $4.65*10^4$ at 1.064 μm with a large core of 50 μm, and it remains $>1*10^4$ with the fault tolerance proportion of tubes size less than 20%, which can increase the flexibility of fiber fabrication. And this point hasn't been mentioned in others single-mode NC-HCFs. Besides, polarization-maintaining transmission with an ultra-low confinement loss of 0.005 dB/m and birefringence of $1.38*10^{-5}$ is achieved by optimizing refractive index of the two

Manuscript received September 5, 2021; revised November 9, 2021; accepted December 16, 2021. Date of publication December 21, 2021; date of current version January 20, 2022. This work was supported by the National Natural Science Foundation of China under Grant 61905080. *(Corresponding author: Yingbin Xing.)*

The authors are with the Wuhan National Laboratory for Optoelectronics, Huazhong University of Science and Technology, Wuhan, Hubei 430000, China (e-mail: yyzhou@hust.edu.cn; caort@hust.edu.cn; wangshijie@hust.edu.cn; jgpeng@mail.hust.edu.cn; lhq@mail.hust.edu.cn; ybc@hust.edu.cn; xingyb@hust.edu.cn; dainl@hust.edu.cn; ljy@hust.edu.cn).

Digital Object Identifier 10.1109/JPHOT.2021.3136895

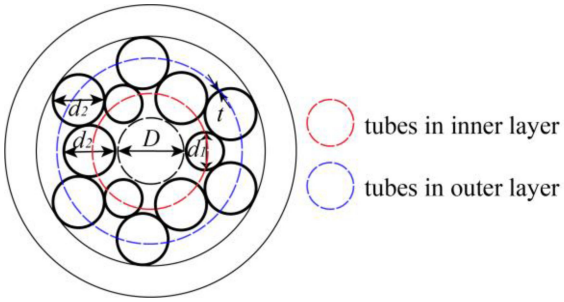

Fig. 1. Cross-section of the proposed fiber.

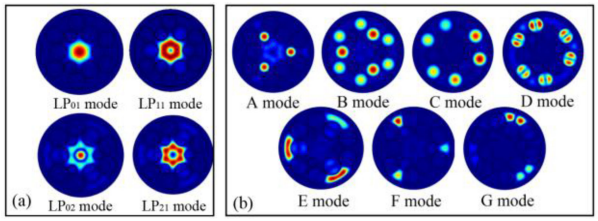

Fig. 2. The electric field intensity distribution on the fiber cross-section of the proposed NC-HCF. (a) the core modes LP_{01}, LP_{11}, LP_{02}, and LP_{21}, (b) cladding modes: A, B, and C modes are the three kinds of like-LP_{01} modes in different kinds of tubes. E and F modes are the like-LP_{01} modes in different kinds of interstices. D and G modes are the like-LP_{11} modes in the tubes and large interstices respectively.

transverse glass tubes without changing the geometry structure. This is the first birefringent negative-curvature hollow-core fiber with a loss below 0.01 dB/m in the 1 μm wavelength window.

II. Structure and Performance

A. Structure Calculation

Fig. 1 shows the cross-section of the proposed NC-HCF. The cladding is constituted of 3 small tubes with diameter of d_1, and 9 large tubes with diameter of d_2. The 3 small tubes and 3 large tubes are arranged in a staggered pattern in the inner layer to form double trigonal-symmetrical anti-resonant elements, while the other 6 large tubes are connected to the jacket tube in the outer layer. The core diameter is D. The thickness of cladding tubes t is set as 0.9 μm. In this work, we use a commercial finite element mode solver (COMSOL) to get all numerical analyses with extremely fine mesh sizes of $\lambda/6$ and $\lambda/4$ in the silica walls and air regions respectively [16], and all simulation results are obtained by adding a perfectly-matched layer (PML) using.

The electric field intensity distribution on the fiber cross-section of fiber core modes and cladding modes of the proposed NC-HCF is shown in Fig. 2. The core modes LP_{01}, LP_{11}, LP_{02}, and LP_{21} as shown in Fig. 2(a). An important characteristic and advantage of the proposed structure is that it can form a rich variety of cladding modes, which are limited in cladding tubes or the interstices between the jacket wall and cladding tubes walls as shown in Fig. 2(b). The 3 small tubes and 3 large tubes in the inner layer can form two kinds of like-LP_{01} modes in tubes, labeled as A mode and B mode respectively. The like-LP_{01} modes and the like-LP_{11} modes in the outer 6 large tubes are labeled as C mode and D mode respectively. In addition, the E mode and F mode are the like-LP_{01} modes in the large interstices and small one between the jacket wall and cladding tubes walls, and the G mode is the like-LP_{11} modes in the large interstices. In the following work, we analyze the coupling between core modes and these cladding modes and study the influence of the size of cladding tubes on the coupling behavior.

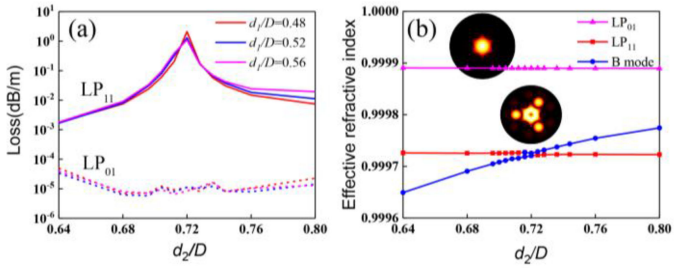

Fig. 3. The coupling behavior of LP_{01} mode and LP_{11} mode. (a) the confinement loss of LP_{01} mode and LP_{11} mode at three different d_1/D, in which the solid and dotted lines are LP_{11} mode and LP_{01} mode respectively, (b) effective refractive index at $d_1/D = 0.48$.

Firstly, we discuss the coupling behavior of LP_{01} mode and LP_{11} mode in the fiber core. The D and t are fixed at 50 μm and 0.9 μm respectively. Fig. 3(a) shows the confinement loss of LP_{01} mode and LP_{11} mode changing with d_2/D when d_1/D is set as 0.48, 0.52 and 0.56 respectively, and Fig. 3(b) shows the effective refractive indices of relative modes at $d_1/D = 0.48$. In Fig. 3(a), the confinement loss of LP_{01} fluctuates in a small range between 10^{-5} dB/m and 10^{-6} dB/m as the dotted lines shown, and there is a wide loss peak of LP_{11} mode at $d_2/D = 0.72$ as the solid lines shown. In Fig. 3(b), the effective refractive index of LP_{01} and LP_{11} mode is unchanged with the increase of d_2/D, while it of B mode continuously increases and the avoided crossing occurs between the effective refractive indices of LP_{11} mode and B mode at $d_2/D = 0.72$, where the LP_{11} mode is coupling strongly with the cladding modes B and the loss of LP_{11} mode reaches the peak [31].

Next, the coupling behavior of LP_{21} mode and LP_{02} mode in the fiber core is discussed. The confinement loss of LP_{21} mode changing with d_1/D at four different d_2/D is calculated. It can be seen from Fig. 4(a) that there are three loss peaks of LP_{21} modes, among which the first peak moves towards to smaller d_1 and the second moves towards to larger d_1 with the increase of d_2, while the position of the third peak remains unchanged. We select two representative values of d_2/D at 0.712 and 0.744 for the following analysis. Fig. 4(c) and Fig. 3(d) show the change of effective refractive index with d_1 at $d_2/D = 0.712$ and $d_2/D = 0.744$ respectively. As shown in Fig. 4(c), when $d_2/D = 0.712$, the LP_{21} mode intersects with E, F at $d_1/D = 0.482$, 0.534 respectively and has an avoided crossing with A modes at $d_1/D = 0.558$, which correspond to the three peaks in Fig. 4(a). Similarly, in Fig. 4(d), when $d_2/D = 0.744$, LP_{21} mode intersects with E, F at $d_1/D = 0.45$, 0.545 respectively and avoids crossing with A modes at $d_1/D = 0.558$, which is very close to the second intersection point *at* 0.545, so the corresponding loss peaks are merged into one peak in Fig. 4(a). By comparing Fig. 4(c) and Fig. 4(d), it can be found that with

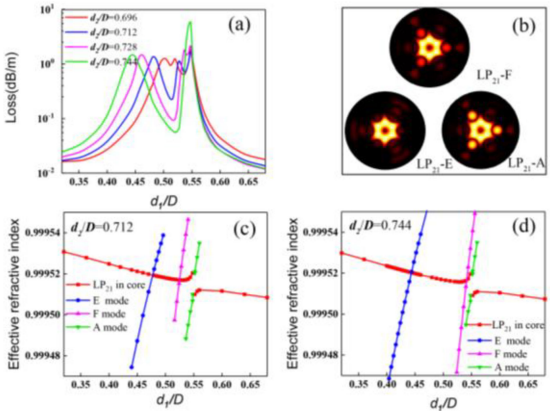

Fig. 4. The coupling behavior between core mode LP_{21} and cladding modes. (a) the confinement loss of LP_{21} mode change with d_1/D at four different d_2/D, (b) the distribution of electric field intensity on the fiber cross-section when LP_{21} mode is coupling with E, F, A mode respectively. (c) effective refractive index at $d_2/D = 0.712$ and (d) $d_2/D = 0.744$.

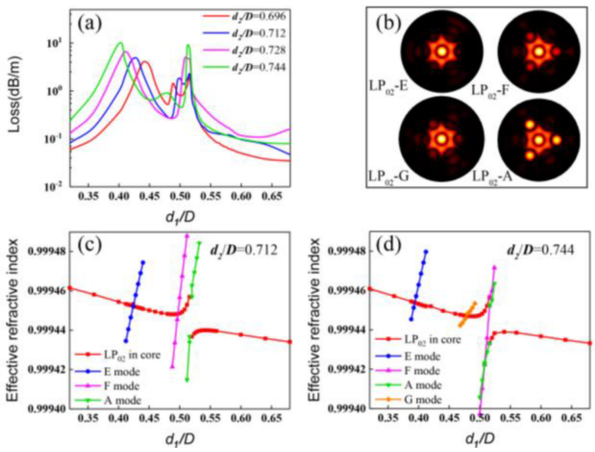

Fig. 5. The coupling behavior between core mode LP_{02} and cladding modes. (a) the confinement loss of LP_{02} mode at four different d_2/D, (b) the distribution of electric field intensity on the fiber cross-section when LP_{02} mode is coupling with E, F, G, A mode respectively. (c) effective refractive index at $d_2/D = 0.712$ and (d) $d_2/D = 0.744$.

the increase of d_2, the intersection of LP_{21} and E mode moves to the smaller d_1, while that of F mode moves to the larger d_1, which is also consistent with the movement direction of the loss peaks in Fig. 4(a). Finally, Fig. 4(b) shows the distribution of electric field intensity on the fiber cross-section when LP_{21} mode is coupling with E, F, A mode, respectively.

The coupling behavior of LP_{02} mode in Fig. 5 is similar to that of LP_{21} mode because the effective refractive indices of them are close. The difference is that when $d_2/D = 0.744$, a new loss peak appears in Fig. 5(a), corresponding to the intersection of LP_{02} with another cladding mode G at $d_1/D = 0.48$. As shown in Fig. 3(b), Fig. 4(b) and Fig. 5(b), the coupling between core modes and E, F, G mode is much weaker than that of A and B mode. It's possibly because comparing with the modes in inner cladding tubes (A, B mode), the modes in the interstices (E, F, G mode) are relatively far from the core modes, so the avoided crossings only occur when the core modes are coupled to the A and B mode, while crossings occur when they are

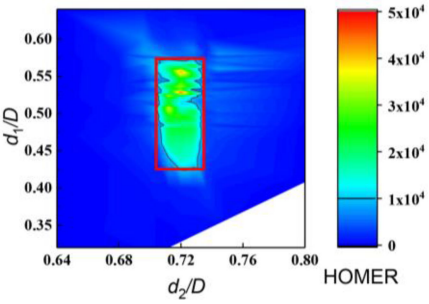

Fig. 6. HOMER as function of d_1/D and d_2/D, the solid red line is the contour line of HOMER $= 1*10^4$.

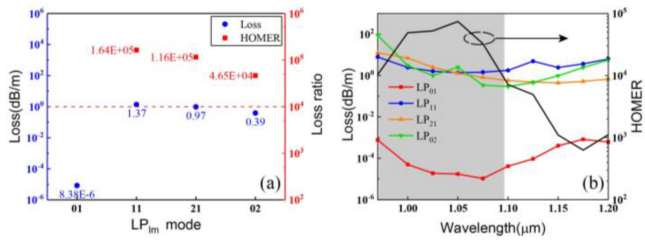

Fig. 7. The confinement loss and loss ratio of core modes at 1.064 μm (a), The bandwidth of confinement loss and the HOMER (b).

coupled to E, F, G mode. However, all of these coupling ways can enhance the confinement loss of correlative core modes as above calculations show.

It can be seen that in a large range of d_1/D and d_2/D, LP_{21} and LP_{02} have multiple loss peaks. In order to find the optimal structure size, we calculate the loss of HOMs and FM when d_1/D ranges from 0.44 to 0.57 and d_2/D ranges from 0.7 to 0.73, and then find out the best single-mode performance. In this work, the single-mode performance is identified by the higher-order modes extinction ratio (HOMER), which is defined as the minimum loss ratio between HOMs and FM [16], [32]. It should be noted that in NC-HCFs, LP_{11} mode is not always the first-lowest loss mode among HOMs and the HOMER generally takes the first four HOMs into consideration. Here only the first three HOMs are discussed because the loss of LP_{31} mode and other HOMs are always higher than the minimum loss between LP_{11}, LP_{21} and LP_{02} modes in the proposed fiber. Fig. 6 shows the HOMER with different d_1/D and d_2/D. The HOMER remains larger than $1*10^4$ as shown in the red frame. And there is the largest HOMER at $d_1/D = 0.53$, $d_2/D = 0.72$.

B. Performance

Fig. 7(a) shows the confinement loss of the four core modes, as well as the loss ratio between the first three HOMs and FM at the wavelength of 1.064 μm when $D = 50$ μm, $d_1/D = 0.53$, $d_2/D = 0.72$. The confinement loss of LP_{01} mode is as low as $8.38*10^{-6}$ dB/m and the HOMER is $4.65*10^4$ with the lowest loss of LP_{02} mode. It is the highest HOMER among all NC-HCFs have reported to the best of our knowledge. Next, In Fig. 7(b), the confinement loss of LP_{01} mode remains below 1 dB/km and HOMER stays larger than $1*10^4$ in the grey area. Furthermore,

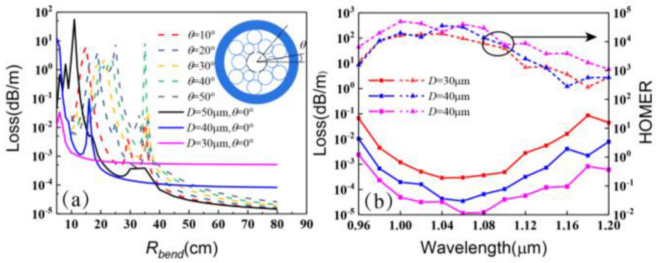

Fig. 8. (a) Dependence of the confinement loss on R_{bend}, the dotted lines represent different bending directions at $D = 50$ um, solid lines represent different core sizes at $\theta = 0$, (b) The confinement loss and HOMER in the 1 μm wavelength window with different core sizes.

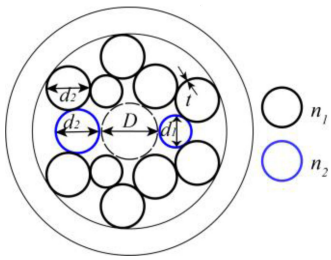

Fig. 9. Cross-section of the proposed PM-NC-HCFs.

the HOMER maintains larger than 1∗103 in a wider range of 0.97 μm ∼1.17 μm. The excellent single mode performance and ultra-low loss of FM make the proposed fiber a potential option for transmitting high-power single mode lasers.

Fig. 8(a) shows the bending performance of the proposed fiber. The bending radius are defined as R_{bend}, and bending direction is identified by the angle θ as Fig. 8(a) shown. The solid lines show the bending loss at different core diameters. We can see that the larger the diameter, the more sensitive the fiber is to bending. When $D = 50$ μm, the loss increases sharply within R_{bend} less than 40cm. When $D = 30$ μm, the R_{bend} can be reduced to less than 10cm. The dotted line describes the loss values in different bending directions at $D = 50$ μm. There are some differences in the loss in different bending directions, but generally, the loss starts to increase sharply when R_{bend} is small to 40cm. Fig. 8(b) shows the loss performance and single-mode performance in the 1 μm wavelength window with different core sizes. The prosed fiber structure has a large HOMER around $1*10^4$ and a fundamental mode loss <1 dB/km at different core diameters in the wavelength of 1.0–1.1 μm, therefore different fiber sizes can be flexibly selected according to loss requirements and bending limits in practical application.

C. Polarization-Maintaining Function Expansion

A novel polarization-maintaining NC-HCF (PM-NC-HCF) based on the originally proposed structure (in Fig. 1) for polarization-sensitive fiber laser systems is put forward. As shown in Fig. 9, the two inner cladding tubes on the transverse are replaced with high-index glass tubes, and the geometry structure stays unchanged. When $D = 50$ μm, $d_1/D = 0.53$, $d_2/D = d_3/D = 0.72$, we consider the refractive indexes of original silica glass

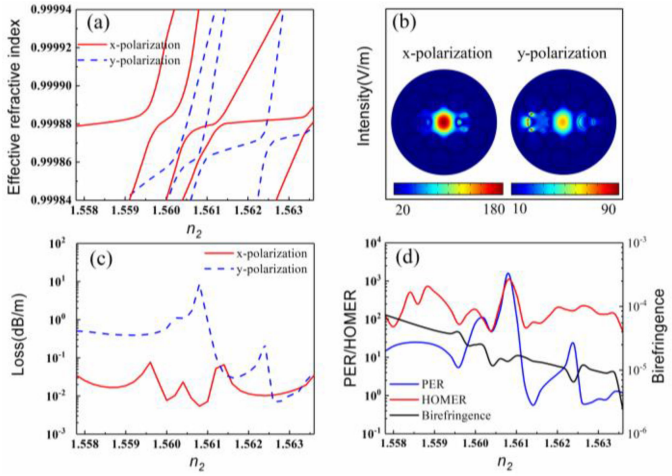

Fig. 10. (a) Effective refractive index and (c) confinement loss of fundamental modes in the x- and y- polarizations changing with the n_2. (b) The electric field intensity distributions of fundamental modes in the x- and y- polarizations respectively, (d) the PER, HOMER and birefringence as a function of n_2.

and high-index glass as n_1 and n_2 respectively. The n_1 is fixed at 1.45 at 1.064 μm in the following study. The most important properties of PM-NC-HCFs are birefringence, loss, polarization extinction ratio (PER), and HOMER in the design process. The PER is defined as the loss ratio of the confinement loss of the y-polarized FM to the x-polarized FM [33], [34].

Fig. 10(a) shows the effective refractive indices of the x- and y-polarized FMs as a function of n_2. There are several avoided crossings when n_2 increases from 1.5578 to 1.5636. The corresponding loss of the fundamental core mode in both x- and y- polarization are shown in Fig. 10(c), where the several loss peaks are corresponding to the avoided crossings in Fig. 10(a).

As shown in Fig. 10(d), the PER and HOMER reach up to 1590 and 1100 respectively while $n_2 = 1.5608$. Then the birefringence is $1.38*10^{-5}$ and the loss of x-polarized FM is only 0.005 dB/m, which is the lowest loss of PM-NC-HCFs as reported before to the authors' knowledge. The electric field intensity distributions of FMs in the x- and y- polarizations at $n_2 = 1.5608$ are displayed in Fig. 10(b), where the y-polarized FM is strongly coupled to the glass modes in the high-index glass, while the coupling of x-polarized FM is much weaker. It is well-known that if PER and HOMER are both larger than 100, it can be regarded as absolute single polarization and single mode guidance in fibers [34]. Therefore, the proposed fiber exhibits a good single-mode and single polarization performance when $n_2 = 1.5608$.

III. Discussion

A. Fabrication Flexibility

It is quite difficult to precisely control both the thickness and the diameter of the cladding tubes during the fabrication process simultaneously. It is also impossible for the tubes to be perfectly tangent to each other as desired, contact interfaces will occur during the fabrication process. It is necessary to discuss the effect of the structural details on the performance. Next,

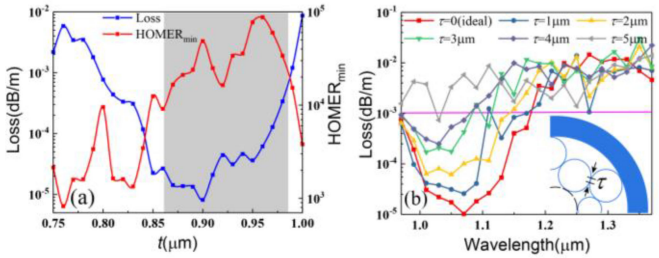

Fig. 11. (a) The confinement loss and HOMER as function of t, (b) The confinement loss as a function of the contact length of nodes τ.

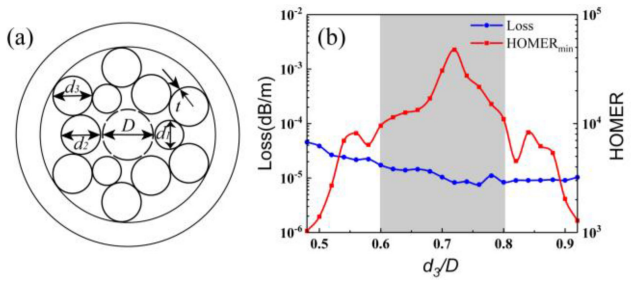

Fig. 12. (a) Cross-section of the proposed NC-HCFs with d_3, (b) The confinement loss of FM and HOMER as function of d_3/D.

we discuss how the thickness of dielectric tube wall, contact length of the nodes and diameter of cladding tubes affect the confinement loss of FM and single-mode performance of the proposed fiber. Fig. 11(a) shows the change of loss and HOMER with the thickness t. The loss of LP_{01} mode remains below 1 dB/km and HOMER remains larger than $1*10^4$ in the grey shaded area with a range around 0.13 μm. It means that the thickness of the cladding tubes should be control accurately in fiber fabrication. The glass nodes are unavoidable in the fiber structure we proposed, and the glass modes in the nodes are coupled with the core modes leading to the increase of fiber loss [35]. As can be seen from the Fig. 11(b), the confinement loss of FM increases, and the bandwidth reduces gradually with the contact length of nodes τ increasing. The confinement loss of FM is still lower than 1 dB/km within a 100nm bandwidth when the node length is less than 4 μm. In addition, the tubes in the inner layer and outer layer are arranged in a staggered pattern, and two kind of tubes support each other to help maintain a uniform gap and position between the anti-resonance elements, which ensures structural uniformity over long distances [36].

Finally, we slightly adjust the diameter of the outer 6 tubes to d_3 as shown in Fig. 12(a). When $d_1/D = 0.53$ and $d_2/D = 0.72$, the influence of d_3/D on the confinement loss of FM and HOMER is demonstrated in Fig. 12(b). The confinement loss of FM is decreased gradually from 10^{-5} dB/m to 10^{-6} dB/m with the increasing of d_3. Notably, the HOMER is larger than $1*10^4$ over a wide range of d_3/D from 0.6 to 0.8, with a fault tolerance range of 10 μm (fault tolerance proportion of 20%), and HOMER is larger than $1*10^3$ over a whole range of calculations. The HOMER reaches its maximum at $d_3/D = 0.72 = d_2/D$, where the structure is the same as we discussed above. And d_1 and d_2 have a fault tolerance range of 6.5 μm and 1.5 μm respectively according to the Fig. 6.

TABLE I
PERFORMANCE COMPARISON BETWEEN SIMULATION RESULTS FROM NC-HCFS AND PM-NC-HCFS REPORTED

Reference		Loss (dB/km)	HOMER	η	Birefringence
NC-HCFs	[37]	1	~2500	~3.2% (HOMER>10^3)	-
	[21]	<0.01	~37000	~6% (HOMER>10^4)	-
	[22]	0.52	12000	~3% (HOMER>10^4)	-
	This work	0.008	46500	20% (HOMER>10^4)	-
PM-NC-HCFs	[23]	20	-	-	$1.3*10^{-5}$
	[33]	<1000	>1000	-	$>10^{-4}$
	[32]	48	495	-	$\sim10^{-5}$
	This work	5	1100	-	$1.38*10^{-5}$

B. Performance Comparison

The comparisons of the simulated properties between the fibers in this work and several single mode NC-HCFs and PM-NC-HCFs reported are shown in Table I, including the contrasts of confinement loss, HOMER, and birefringence. In addition, we define the largest fault tolerance proportion of fiber cladding structure as η, which is estimated according to the data graphs and structures in these papers. As shown in Table I, comparing with other NC-HCFs, the HOMER in this work is the highest one, and diameters with a fault tolerance range of 10 μm ($\eta = 20\%$) can be achieved in our structure, whereas η of other structures are all below 10%. In cases where the thickness of tubes should be controlled accurately, a larger η means more flexibility for the fiber fabrication. Comparing with other PM-NC-HCFs, the confinement loss of the fiber proposed in this work is reduced by order of magnitude. On the other hand, the PER and HOMER of our structure are both larger than 1000, guaranteeing the single-mode and single-polarization transmission for high-power laser delivery at 1.064 μm. This is the first PM-NC-HCF with a loss below 0.01 dB/m in the 1 μm wavelength window.

IV. CONCLUSION

In conclusion, we proposed a novel negative-curvature hollow-core fiber with double trigonal-symmetrical anti-resonant elements implementing single-mode or polarization-maintaining transmission for high-power laser delivery at the 1 μm wavelength window. In this fiber structure, the core is evenly surrounded by tubes with two different sizes forming a rich variety of cladding modes to couple with high-order modes in fiber core, and thereby achieving the best single-mode performance with a minimum higher-order modes extinction ratio (HOMER) as high as $4.65*10^4$. The HOMER remains $>1*10^4$ with the confinement loss $<1*10^{-5}$ dB/m

within a large fault tolerance proportion of tubes size, which will enhance the flexibility of fiber fabrication. Finally, by optimizing refractive index of the two transverse glass tubes without changing the geometry structure, it achieves polarization-maintaining transmission with an ultra-low confinement loss of 0.005 dB/m, which is the lowest loss of PM-NC-HCFS in the 1 μm wavelength window to the authors' knowledge. Meanwhile, the birefringence is $1.38*10^{-5}$ with the high PER and the HOMER (both >1000), promising the absolute single-mode and polarization-maintaining transmission for polarization-sensitive fiber laser systems.

REFERENCES

[1] V. Fomin, V. Gapontsev, E. Shcherbakov, A. Abramov, A. Ferin, and D. Mochalov, "100 kW CW fiber laser for industrial applications," in *Proc. Int. Conf. Laser Opt.*, 2014, pp. 1–1.

[2] Y. Takubo, S. Ikoma, K. Uchiyama, H. Kusaka, Y. Umeda, and M. Kashiwagi, "Dynamic analysis of materials processing with 5-kW single-mode fiber laser," in *Fiber Lasers XVI: Technol. Syst.*, vol. 1089712, 2019, Art. no. 37.

[3] G. P. Agrawal, *Nonlinear Fiber Optics*, San Francisco, CA, USA: Academic, 2001.

[4] F. Poletti *et al.*, "Towards high-capacity fibre-optic communications at the speed of light in vacuum," *Nat. Photon.*, vol. 7, no. 4, pp. 279–284, 2013.

[5] P. S. J. Russell, P. Hölzer, W. Chang, A. Abdolvand, and J. C. Travers, "Hollow-core photonic crystal fibres for gas-based nonlinear optics," *Nat. Photon.*, vol. 8, no. 4, pp. 278–286, 2014.

[6] C. M. Harvey, F. Yu, J. C. Knight, W. J. Wadsworth, and P. Almeida, "Reducing nonlinear limitations of ytterbium mode-locked fibre lasers with hollow-core negative curvature fibre," in *Proc. Conf. Lasers Electro-Opt. Eur. - Tech. Dig.*, 2015, pp. 20–21.

[7] D. C. Jones, C. R. Bennett, M. A. Smith, and A. M. Scott, "High-power beam transport through a hollow-core photonic bandgap fiber," *Opt. Lett.*, vol. 39, no. 11, pp. 3122–3125, 2014.

[8] R. Amezcua-Correa, F. Gérôme, S. Leon-Saval, N. G. R. Broderick, T. A. Birks, and J. C. Knight, "Control of surface modes in low loss hollow-core photonic bandgap fibers," *Opt. Exp.*, vol. 16, no. 2, pp. 1142–1149, 2008.

[9] G. T. Jasion *et al.*, "Hollow core NANF with 0.28 dB/km attenuation in the c and l mands," in *Proc. Opt. Fiber Commun. Conf. Exhib.*, 2020, pp. 3–5.

[10] W. DIng, Y. Y. Wang, S. F. Gao, M. L. Wang, and P. Wang, "Recent progress in low-loss hollow-core anti-resonant fibers and their applications," *IEEE J. Sel. Top. Quantum Electron.*, vol. 26, no. 4, Aug. 2020, Art. no. 4400312.

[11] B. Beaudou *et al.*, "MilliJoule laser pulse delivery for spark ignition through kagome hollow-core fiber," *Opt. Lett.*, vol. 37, no. 9, pp. 1430–1432, 2012.

[12] S. A. Mousavi *et al.*, "Nonlinear dynamic of picosecond pulse propagation in atmospheric air-filled hollow core fibers," *Opt. Exp.*, vol. 26, no. 7, pp. 8866–8882, 2018.

[13] J. D. Shephard *et al.*, "Silica hollow core microstructured fibers for beam delivery in industrial and medical applications," *Front. Phys.*, vol. 3, no. 24, pp. 1–11, 2015.

[14] M. Cassataro *et al.*, "Generation of broadband mid-IR and UV light in gas-filled single-ring hollow-core PCF," *Opt. Exp.*, vol. 25, no. 7, pp. 7637–7644, 2017.

[15] Y. P. Yatsenko *et al.*, "Multiband supercontinuum generation in an air-core revolver fibre," *Quantum Electron.*, vol. 47, no. 6, pp. 553–560, 2017.

[16] F. Poletti, "Nested antiresonant nodeless hollow core fiber," *Opt. Exp.*, vol. 22, no. 20, pp. 23807–23828, 2014.

[17] L. Vincetti and V. Setti, "Waveguiding mechanism in tube lattice fibers," *Opt. Exp.*, vol. 18, no. 22, pp. 23133–23146, 2010.

[18] N. M. Litchinitser, A. K. Abeeluck, C. Headley, and B. J. Eggleton, "Antiresonant reflecting photonic crystal waveguides," *Opt. Lett.*, vol. 27, no. 18, pp. 1592–1594, 2002.

[19] B. Debord *et al.*, "Ultralow transmission loss in inhibited-coupling guiding hollow fibers," *Optica*, vol. 4, no. 2, pp. 209–217, 2017.

[20] B. Debord *et al.*, "Hypocycloid-shaped hollow-core photonic crystal fiber Part I: Arc curvature effect on confinement loss," *Opt. Exp.*, vol. 21, no. 23, pp. 28597–28608, 2013.

[21] M. I. Hasan, N. Akhmediev, and W. Chang, "Positive and negative curvatures nested in an antiresonant hollow-core fiber," *Opt. Lett.*, vol. 42, no. 4, pp. 703–706, 2017.

[22] S. Habib, E. Antonio-lopez, C. Markos, A. Schülzgen, and R. Amezcua-correa, "Single mode, low-loss 5-tube nested hollow-core anti-resonant fiber," in *Proc. Opt. Fiber Commun. Conf.*, 2019, pp. 12–14.

[23] C. Wei, C. R. Menyuk, and J. Hu, "Polarization-filtering and polarization-maintaining low-loss negative curvature fibers," *Opt. Exp.*, vol. 26, no. 8, pp. 9528–9540, 2018.

[24] S. Yan, Z. Lian, S. Lou, X. Wang, W. Zhang, and Z. Tang, "A new method to achieve single-polarization guidance in hollow-core negative-curvature fibers," *IEEE Access*, vol. 8, pp. 53419–53426, 2020.

[25] I. M. Ankan, M. A. Mollah, A. K. Paul, and K. Chakrabarti, "Polarization-maintaining and polarization-filtering negative curvature hollow core fiber in THz regime," in *Proc. Region 10 Symp.*, 2020, pp. 612–615.

[26] G. Stępniewski, D. Dobrakowski, D. Pysz, R. Kasztelanic, R. Buczyński, and M. Klimczak, "Birefringent large-mode-area anti-resonant hollow core fiber in the 19 μm wavelength window," *Opt. Lett.*, vol. 45, no. 15, pp. 4280–4283, 2020.

[27] W. Ding and Y.-Y. Wang, "Hybrid transmission bands and large birefringence in hollow-core anti-resonant fibers," *Opt. Exp.*, vol. 23, no. 16, pp. 21165–21174, 2015.

[28] Zhao X *et al.*, "High birefringence, single-polarization, low loss hollow-core anti-resonant fibers," *Opt. Exp.*, vol. 29, no. 22, pp. 36273–36286, 2021.

[29] M. Wu, B. Li, J. Li, G. Zhou, C. Xia, and Z. Hou, "Research on fabrication and performance of hollow-core anti-resonant fiber coated with copper film," *IEEE Photon. J*, vol. 12, no. 3, 2020, Art. no. 7101708.

[30] C. Wei, R. Joseph Weiblen, C. R. Menyuk, and J. Hu, "Negative curvature fibers," *Adv. Opt. Photon.*, vol. 9, no. 3, pp. 504–561, 2017.

[31] M. Selim Habib, C. Markos, and R. Amezcua-Correa, "Impact of cladding elements on the loss performance of hollow-core anti-resonant fibers," *Opt. Exp.*, vol. 29, no. 3, pp. 3359–3374, 2021.

[32] S. Yan, S. Lou, Z. Lian, W. Zhang, and X. Wang, "Tunable single-polarization single-mode negative-curvature fiber with an asymmetrical refractive index cladding for mid-infrared region," *J. Lightw. Technol.*, vol. 37, no. 22, pp. 5707–5713, 2019.

[33] J. Tu *et al.*, "Chalcogenide-glass nested anti-resonant nodeless fibers in mid-infrared region," *J. Lightw. Technol.*, vol. 36, no. 22, pp. 5244–5253, 2018.

[34] A. N. Kolyadin, A. F. Kosolapov, A. D. Pryamikov, A. S. Biriukov, V. G. Plotnichenko, and E. M. Dianov, "Light transmission in negative curvature hollow core fiber in extremely high material loss region," *Opt. Exp.*, vol. 21, no. 8, pp. 9514–9519, 2013.

[35] M. B. S. Nawazuddin *et al.*, "Lotus-shaped negative curvature hollow core fiber with 10.5 dB/km at 1550 nm wavelength," *J. Lightw. Technol.*, vol. 36, no. 5, pp. 1213–1219, 2018.

[36] M. S. Habib, O. Bang, and M. Bache, "Low-loss hollow-core silica fibers with adjacent nested anti-resonant tubes," *Opt. Exp.*, vol. 23, no. 13, pp. 17394–17406, 2015.